Electrohydrodynamic instability of miscible core–annular flows with electrical conductivity stratification

Zijing Ding[1],† and Teck Neng Wong[1],†

[1]School of Mechanical and Aerospace Engineering, Nanyang Technological University,
Singapore 639798, Singapore

This paper investigates the electrohydrodynamical instability of two miscible flows in a micro-pipe subject to an axial electric field. There is an electrical conductivity stratification between the two layers. A weak shear flow arises from a constant axial pressure gradient. The three-dimensional linear stability analysis is studied under the assumption of a quasi-steady state. The influences of the conductivity ratio η, the interface location a, the interface thickness δ, the Reynolds number Re and the Schmidt number Sc on the linear stability of the flows are investigated. The flow becomes more unstable for a larger conductivity contrast. When the conductivity in the inner layer is larger, the critical unstable mode can be dominated by either the corkscrew mode (the azimuthal wavenumber $m = 1$) or the axisymmetric mode ($m = 0$), which is dependent on the interface location a. It is observed that, when the interface is proximal to pipe's wall, the critical unstable mode shifts from the corkscrew mode to the axisymmetric mode. When the conductivity is larger in the outer layer, the instability is dominated by the axisymmetric mode. A detailed parametric study shows that the flow is least stable when the interface between the two liquids is located at approximately $a = 0.3$ and $a = 0.2$ for conductivity ratios of $\eta = 0.5$ and $\eta = 2$ respectively. The flow becomes more stable as the interface becomes thicker, and the shear flow and ionic diffusion are found to have a stabilizing effect due to the enhancement of dissipation mechanisms.

Key words: instability, MHD and electrohydrodynamics, micro-/nano-fluid dynamics

1. Introduction

For many years, electrohydrodynamics has attracted extensive research due to its wide applications in microfluidic devices, such as in ink jetting, drug delivery and chemical analysis. One favourable application of the use of an electric field is to pump liquids in micro-channels as it will not induce mechanical noise. Another potential use of an electric field is to enhance the mixing in microfluidic devices (Lin 2009). When an external electric field is applied across a liquid layer, the Maxwell stress can initiate flow instability in the liquid layer with spatial changes in the electrical properties. In

† Email addresses for correspondence: zding001@e.ntu.edu.sg, mtnwong@e.ntu.edu.sg.

previous studies, the instability of flow systems could be triggered by an electric field due to abrupt changes (Melcher & Schwartz 1968; Melcher & Smith 1969) or spatial gradients in electrical properties (Melcher & Firebaugh 1967).

In the former case, the liquids are usually assumed to be immiscible and the interfacial instability is of particular interest (Saville 1997; Ozen *et al.* 2006). It is assumed that there is no electrical charge within the bulk region, while electrical charges accumulate on the interface. One such model proposed was the leaky-dielectric model by Taylor (1966). Recently, Wang (2012) discussed the influence of surface charge transportation on the breakup of a poorly conducting liquid thread surrounded by an insulating liquid layer in a radial electric field. Ding, Wong & Li (2013) investigated the instability of two leaky-dielectric co-flows in an annulus duct in a radial electric field. There was an abrupt change in the electrical conductivity as well as the electrical permittivity, such that the Maxwell stress could either enhance or impede the interfacial deformation. Their results demonstrated that the electric field may inhibit the capillary instability caused by surface tension and interfacial wave instability due to viscosity stratification (Ding *et al.* 2013).

The latter study of liquids with spatial electrical property gradients focused on the influence of electrical body force on the stability of electro-convection. The gradients may be caused by non-isothermal heating (Yoshikawa, Crumeyrolle & Mutabazi 2013) or due to the non-uniform distribution of ionic concentration (Lin 2009). To the best of our knowledge, previous studies of electro-convection in a liquid layer with electrical conductivity gradients in an isothermal environment have been focused on flows in a square duct in past decades.

Pioneering work on electro-convection in a planar liquid layer with an electrical conductivity gradient was carried out by Baygents & Baldessari (1998). A wall-normal electric field was imposed between two parallel plates. They proposed that the occurrence of instability was triggered by the dielectrophoretic effect (Baygents & Baldessari 1998). They found that the lower conductivity boundary had a strong stabilizing effect when the conductivity gradient was large. It should be noted that the assumption of exchange of stability made by them was incorrect because the critical unstable mode may be oscillatory (Baygents & Baldessari 1998). Chang, Ruo & Chen (2009) dropped the assumption of exchange of stability and considered the influence of an imposed shear flow wherein the oscillatory and stationary unstable modes were discovered. It was found that the instability could be enhanced by a very weak shear flow, and the transverse mode (zero spanwise wavenumber) became critical rather than the longitudinal model (zero streamwise wavenumber). However, as the shear flow became stronger, they found that the longitudinal mode became critical and the critical mode was independent of the shear flow (Chang *et al.* 2009). Ruo, Chang & Chen (2010) extended the study of Chang *et al.* (2009) and considered the rotating effect. Their results showed that rotation played a stabilizing role in the system while the electric field was the major cause of instability (Ruo *et al.* 2010). Recently, Ding & Wong (2014) investigated the instability of an annular liquid layer with electrical conductivity gradients. Their results showed that the critical unstable mode depended on the geometry of the duct and the critical unstable mode may be either stationary or oscillatory (Ding & Wong 2014).

Unlike the studies of Baygents & Baldessari (1998), Chang *et al.* (2009), Ruo *et al.* (2010) and Ding & Wong (2014), in which the electro-convection was triggered due to a spatial gradient in the electrical conductivity, Lin *et al.* (2004) considered two miscible flows with an electrical conductivity stratification. To achieve such a conductivity stratification flow in experiments, Lin *et al.* (2004) used two

electrolytes with different ionic concentrations. The liquids were pumped into the channel using a syringe pump. A Couette flow arose from a tangential electric field due to the electro-osmosis phenomenon after removing the pressure gradient. The electro-osmosis phenomenon was treated as a slippery boundary condition and the slip velocity was related to the zeta potential in the electrical double layer. However, it should be noted that the electro-osmosis flow was rather weak. They investigated the linear stability by assuming a quasi-steady base flow and verified their results via a direct numerical simulation. A depth-averaged model was proposed by Storey, Lin & Santiago (2005) to investigate the electrohydrodynamical instability in a square pipe. The depth-averaged model simplified the problem to a two-dimensional flow, but showed good agreement with the three-dimensional results (Storey *et al.* 2005). The convective and absolute electrokinetic instability with a conductivity stratification was extended by Chen *et al.* (2005). Chen *et al.* (2005) used aqueous electrolytes of 10:1 conductivity ratio and applied a streamwise electric field. The two-dimensional instability was studied via a thin-layer assumption that the channel width was much larger than the channel depth. Santos & Storey (2008) extended the studies to a flow with streamwise conductivity gradients and investigated the linear instability as well as the nonlinear evolution. Notably, in these studies (Baygents & Baldessari 1998; Chang *et al.* 2009; Ruo *et al.* 2010) non-slippery conditions were adopted, while in other studies (Lin *et al.* 2004; Chen *et al.* 2005; Storey *et al.* 2005; Santos & Storey 2008) a slippery boundary condition was considered. The latter focused on the stability of electro-osmosis flow.

Previously, investigations of the electrohydrodynamical instability of multi-immiscible electrolyte flows in a circular pipe have mainly focused on the interfacial instability. Georgiou *et al.* (1991) investigated the influence of an electro-double-layer on the long-wave instability of a core–annular electrolyte film. They found that double layer repulsion can impede the capillary instability, while double layer attraction enhances the capillary instability. Extension of such a flow was performed by Conroy *et al.* (2010, 2011, 2012). They considered a two-electrolyte flow in a pipe. The interfacial instability and dynamics were studied in the framework of long-wave theory in which the system was reduced asymptotically (Conroy *et al.* 2010, 2011, 2012). When an axial electric field is applied, most previous studies have been focused on the stability of a liquid jet. Theoretical and experimental studies have shown that the electric field has a stabilizing (Melstel 1996) or destabilizing (Hohman *et al.* 2001) effect in electrified jets. For miscible flows in a circular pipe, we note that previous studies focused on the problem of viscosity stratification flows (Selvam *et al.* 2007; d'Olce *et al.* 2008, 2009). The core–annular flows were driven by two coaxial pumps (Selvam *et al.* 2007; d'Olce *et al.* 2008, 2009). Water–natrosol mixtures were used in experiments which could provide a large viscosity contrast but small variations in densities (Selvam *et al.* 2007; d'Olce *et al.* 2008, 2009). Experiments by d'Olce *et al.* (2008, 2009) demonstrated that perfect core–annular flows can be observed in such flow systems. For a single fluid flow in a circular micro-pipe, experimental study showed that the fluid was laminar and the electro-osmotic moving speed was very small (Sinton & Li 2003). A careful look at the literature indicates that studies on electrohydrodynamic instability of miscible liquid flows in a pipe are very limited. In this paper, our aim is to extend the electrohydrodynamical instability of immiscible flows in a circular pipe to miscible flows. In addition, in micro-channel flows, the Reynolds number is usually very small, therefore mixing due to turbulence will not occur (Sinton & Li 2003). This paper provides a potential method that can facilitate the mixing in a micro-pipe through electrohydrodynamic instability.
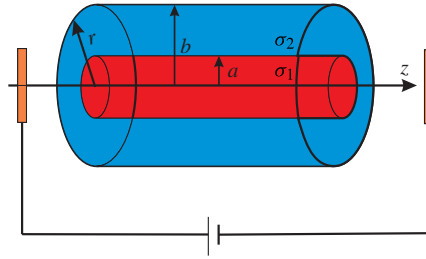
FIGURE 1. (Colour online) The geometry of the system. σ_1 and σ_2 represent the electrical conductivity in the inner and outer layers respectively.

The rest of this paper is organized as follows. In §2, the mathematical formulation is constructed. Section 3 presents the base state and non-dimensional governing system. In §4, the linear stability analysis is implemented and the normal mode analysis is considered. In §5, the energy analysis is carried out to interpret the instability mechanism. Section 6 presents the parametric studies of the dimensionless parameters. In the last section, our conclusion is given.

2. Mathematical formulation

We consider a pipe flow system as shown in figure 1. The radius of the pipe is b. The two liquids are miscible dilute electrolyte solutions. The liquids are Newtonian and the values of the density ρ, kinematic viscosity ν and dynamic viscosity $\mu = \rho\nu$ of the two liquids are assumed to be the same (Lin *et al.* 2004). There is a sharp change in the ionic concentration where the two liquids meet at $r = a$. Therefore, a sharp change in the electrical conductivity occurs at $r = a$. A constant electric field is imposed in the axial direction. A constant pressure gradient is imposed along the axis.

In this paper, the three-dimensional hydrodynamical problem is considered. Cylindrical coordinates (r, θ, z) are chosen; gravity is neglected. The motion of the liquids is governed by the continuity equation and the momentum equation,

$$\nabla \cdot \boldsymbol{v} = 0, \tag{2.1}$$

$$\rho \frac{\mathrm{D}\boldsymbol{v}}{\mathrm{D}t} = -\nabla p + \mu\nabla^2\boldsymbol{v} + \boldsymbol{f}, \tag{2.2}$$

where $\boldsymbol{v} = u\boldsymbol{e}_r + v\boldsymbol{e}_\theta + w\boldsymbol{e}_z$ is the velocity and $\mathrm{D}/\mathrm{D}t = \partial/\partial t + u(\partial/\partial r) + (v/r)(\partial/\partial\theta) + w(\partial/\partial z)$ is the material derivative operator. Here, $\boldsymbol{f}$ is the electrical force which can be related to the Maxwell stress tensor $\boldsymbol{T}^M$ by

$$\boldsymbol{f} = \nabla \cdot \boldsymbol{T}^M. \tag{2.3}$$

Usually, analysis of (2.2) is difficult because the electric field is coupled to the free charge density ρ_e according to Maxwell's equations. Moreover, the free charge density is coupled to the flow field. In this paper, we assume that the electrical current density $\boldsymbol{J}_e$ and the induced current density $(\partial\epsilon\boldsymbol{E}/\partial t)$ are modest, such that the induced magnetic field is negligible. Therefore, the electrostatic problem is considered in this paper,

$$\nabla \times \boldsymbol{E} = 0. \tag{2.4}$$

Hence, the Maxwell stress $\boldsymbol{T}^M = \epsilon\boldsymbol{E}\boldsymbol{E} - (1/2)\epsilon\|\boldsymbol{E}\|^2\boldsymbol{I}$. The parameter ϵ is the dielectric permittivity and $\boldsymbol{E}$ is the electric field. Here, $\|\boldsymbol{E}\|^2 = \boldsymbol{E}\cdot\boldsymbol{E}$ and $\boldsymbol{I}$ is the identity tensor. The charge density is given by Gauss's law,

$$\rho_e = \boldsymbol{\nabla}\cdot(\epsilon\boldsymbol{E}). \tag{2.5}$$

Hence, the momentum equation (2.2) is now written as

$$\rho\frac{\mathrm{D}\boldsymbol{v}}{\mathrm{D}t} = -\boldsymbol{\nabla}p + \mu\nabla^2\boldsymbol{v} + \rho_e\boldsymbol{E} - \frac{1}{2}\|\boldsymbol{E}\|^2\boldsymbol{\nabla}\epsilon. \tag{2.6}$$

In isothermal and dilute electrolyte solution conditions, the electrical permittivity ϵ is approximately that of the solvent (Lin *et al.* 2004). In some non-isothermal conditions, this term $(\|\boldsymbol{E}\|^2\boldsymbol{\nabla}\epsilon)/2$ is crucial since there is a gradient of permittivity due to the non-isothermal condition which causes a circulation flow in the system (Yoshikawa *et al.* 2013). In this paper, we consider isothermal conditions and the electrical permittivity is assumed to be constant for dilute electrolyte solutions. Therefore, the term $(\|\boldsymbol{E}\|^2\boldsymbol{\nabla}\epsilon)/2$ is ignored. In previous studies by Chang *et al.* (2009) and Ding *et al.* (2013), this term $(\|\boldsymbol{E}\|^2\boldsymbol{\nabla}\epsilon)/2$ was also neglected under the assumptions of dilute electrolyte solution and an isothermal environment. The term $\rho_e\boldsymbol{E}$ is called the electrical body force.

Because the electrostatics is considered, the electric field $\boldsymbol{E}$ can be related to the electrical potential by

$$\boldsymbol{E} = -\boldsymbol{\nabla}\phi. \tag{2.7}$$

Hence, Gauss's law (2.5) is expressed by the following Poisson equation:

$$\nabla^2\phi = -\frac{\rho_e}{\epsilon}. \tag{2.8}$$

Conservation of electrical charge gives

$$\frac{\partial\rho_e}{\partial t} + \boldsymbol{\nabla}\cdot\boldsymbol{J}_e = 0. \tag{2.9}$$

In this paper, the electrolyte solution is considered as an ohmic conductor, which means that diffusion of the charge can be neglected. Then, the current density $\boldsymbol{J}_e$ is given by

$$\boldsymbol{J}_e = \sigma\boldsymbol{E} + \rho_e\boldsymbol{v}, \tag{2.10}$$

where σ is the electrical conductivity. Substituting (2.10) into the current conservative law, we obtain

$$\frac{\mathrm{D}\rho_e}{\mathrm{D}t} + \boldsymbol{\nabla}\cdot(\sigma\boldsymbol{E}) = 0. \tag{2.11}$$

Because the electrolyte solution is considered to be an ionic conductor, the conductivity depends on the local ion concentration. Accordingly, the conductivity can be described by the following diffusion equation (Melcher 1981; Baygents & Baldessari 1998; Chang *et al.* 2009):

$$\frac{\mathrm{D}\sigma}{\mathrm{D}t} = K_{eff}\nabla^2\sigma, \tag{2.12}$$

where K_{eff} is an effective diffusivity due to the Brownian motion of the ions. Equation (2.12) is valid if the local electrical time is much shorter than the fluid time and the time for ion electromigration,

$$\frac{\epsilon}{\sigma} \ll \frac{b^2}{\nu} \ll \frac{b}{\omega E} \quad \text{and} \quad \frac{b^2}{\omega k_B T}, \tag{2.13a,b}$$

in which $k_B T$ is the Boltzmann temperature and ω is the characteristic mobility of the charge-carrying solutes. The conditions imply that the ions are carried by a fluid parcel. Typical values of these parameters can be found in Melcher's book (Melcher 1981) and Lin *et al.*'s work (Lin *et al.* 2004): $\epsilon \approx 10^{-10}$ C V^{-1}, $\omega \approx 10^{-8}$ m^2 V^{-1} s^{-1}, kinematic viscosity $\nu \approx 10^{-6}$ m^2 s^{-1}, conductivity $\sigma \approx 10^{-4}$ S m^{-1}, strength of a typical electric field $E = O(10^3)$ V m^{-1} and pipe radius $b = 10^{-3}$ m. A similar form to (2.12) was also derived by Lin *et al.* (2004) from the species conservation law if the electromigration was neglected. Baygents & Baldessari (1998) indicated that the diffusion term $K_{eff} \nabla^2 \sigma$ is responsible for the existence of a threshold electric field and cannot be neglected. This was also mentioned in the following works of Lin *et al.* (2004), Chang *et al.* (2009) and Ding & Wong (2014).

At the initial time, the electrical conductivity in each layer is $\sigma = \sigma_1|_{r<a}$, $\sigma_2|_{a<r<b}$ ($\sigma_1 \neq \sigma_2$). The subscript $i = 1, 2$ denotes the inner layer and outer layer respectively. This can be achieved by using two aqueous electrolytes with different ionic concentrations (Lin *et al.* 2004; Chen *et al.* 2005).

In this paper, we apply the non-slip and non-penetration boundary conditions at $r = b$:

$$u = v = w = 0. \tag{2.14}$$

Here, the basic flow is driven by pressure, and the maximum speed occurring at the centreline is approximately 10^{-4}–10^{-2} m s^{-1}. Usually, the electro-osmosis flow is very weak and the flow velocity can be estimated by the Helmholtz–Smoluchowski formula $U_E = -\epsilon E \zeta / \mu$, where ζ is the zeta potential which is responsible for the electro-osmosis flow. This velocity usually has an order of $O(10^{-6})$ m s^{-1} provided $\zeta = -10^{-2}$ V, $\epsilon = 10^{-10}$ C V^{-1} m^{-1}, $\mu = 10^{-3}$ kg m^{-1} s^{-1} and $E = 10^3$ V m^{-1}. Clearly, the electro-osmotic velocity is much weaker than the pressure driven flow in this paper. Hence, in what follows, the non-slip and non-penetration boundary conditions in (2.14) are applied so that the electro-osmosis phenomenon is neglected.

There is no flux of the ions at $r = b$; therefore,

$$\frac{\partial \sigma}{\partial r} = 0. \tag{2.15}$$

The circular pipe is non-conducting,

$$\frac{\partial \phi}{\partial r} = 0. \tag{2.16}$$

3. Base state and scalings

At the base state, the flow field and the electric field are decoupled because the electrolyte solution is initially neutral, i.e. the net charge density is zero. The flow is driven by a constant pressure gradient $\partial_z \bar{p}$. Therefore, the base velocity profile is

$$\bar{w} = \frac{\partial_z \bar{p}}{4\mu}(r^2 - b^2). \tag{3.1}$$

We assume that the interface between the two liquids has grown diffusively to a finite thickness δ. Moreover, we assume that the diffusion is sufficiently slow to allow us to employ a quasi-steady base state for the linear stability analysis. Provided $\delta \ll 1$, the profile of the conductivity can be approximated by the error function:

$$\bar{\sigma} = \frac{\sigma_1 + \sigma_2}{2} + \frac{\sigma_2 - \sigma_1}{2} \text{erf}\left(\frac{r-a}{\delta}\right). \tag{3.2}$$

Equation (3.2) was used by Selvam *et al.* (2007) in their study to describe the profile of the viscosity of a viscosity stratified flow in a circular pipe.

The base electrical conductivity profile can also be obtained via solution of the following equation (Lin *et al.* 2004):

$$\frac{\partial \sigma}{\partial t} = K_{eff}\left(\frac{\partial^2 \sigma}{\partial r^2} + \frac{1}{r}\frac{\partial \sigma}{\partial r}\right). \tag{3.3}$$

In experiments, K_{eff} ranges from 10^{-9} to 10^{-12} m^2 s^{-1}.

The charge density ρ_e is zero, and the electric field exists only in the axial direction. This gives the base state of the electrical potential:

$$\bar{\phi} = \phi_0 - Ez, \tag{3.4}$$

where E is the strength of the imposed electric field and ϕ_0 is the reference electrical potential.

Taking the velocity scale $W = -(\partial_z \bar{p} b^2)/4\mu$, the length scale b, the time scale b/W, the pressure scale ρW^2, the electrical potential scale Eb and the conductivity scale $\sigma_2 - \sigma_1$, we non-dimensionalize the system (2.1)–(2.16):

$$\nabla \cdot \mathbf{v} = 0, \tag{3.5}$$

$$\frac{D\mathbf{v}}{Dt} = -\nabla p + \frac{1}{Re}\nabla^2 \mathbf{v} + \frac{Q}{Re^2 Sc}\nabla^2 \phi \nabla \phi, \tag{3.6}$$

$$\frac{1}{R_t}\frac{D(\nabla^2 \phi)}{Dt} + \nabla \cdot \{[(\eta - 1)\sigma + 1]\nabla \phi\} = 0, \tag{3.7}$$

$$\frac{D\sigma}{Dt} = \frac{1}{ReSc}\nabla^2 \sigma, \tag{3.8}$$

where $Re = \rho Wb/\mu$ is the Reynolds number, $Q = (\epsilon E^2 b^2/\mu K_{eff})$ is the scaled electrical energy and is defined as the electrical number in this paper, $\eta = \sigma_2/\sigma_1$ denotes the conductivity ratio and $Sc = \nu/K_{eff}$ is the electrical Schmidt number. Baygents & Baldessari (1998) proposed that $Sc \in [10^3, 10^6]$. In the study of Chang *et al.* (2009), Sc was assumed to vary in $[10^2, 10^5]$. The parameter $R_t = (d/W)/(\epsilon/\sigma_1)$ measures the ratio of fluid time to electrical time. We assume that R_t is very large so that the electric time is significantly smaller than the fluid time. Therefore, (3.7) can be simplified to

$$[(\eta - 1)\sigma + 1]\nabla^2 \phi + (\eta - 1)\nabla \sigma \cdot \nabla \phi = 0. \tag{3.9}$$

The dimensionless boundary conditions at $r = 1$ are

$$u = v = w = \frac{\partial \sigma}{\partial r} = \frac{\partial \phi}{\partial r} = 0. \tag{3.10}$$
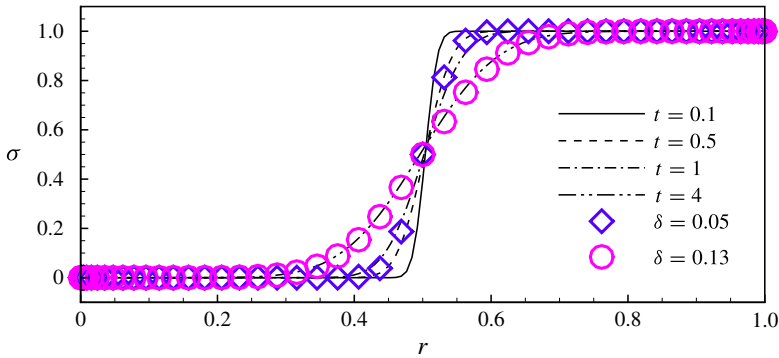
FIGURE 2. (Colour online) The base electrical conductivity profile. The lines are obtained by numerical experiments on the dimensionless form of (3.3) and the circles and diamonds are obtained from the error function (3.12). The relevant parameters are $a = 0.5$, $ReSc = 1000$.

The dimensionless base state is defined as follows:

$$\bar{w} = 1 - r^2, \tag{3.11}$$

$$\bar{\sigma} = \frac{1}{2} + \frac{1}{2}\mathrm{erf}\left(\frac{r - a}{\delta}\right), \tag{3.12}$$

$$\bar{\phi} = -z, \tag{3.13}$$

in which a is scaled on the length scale b which falls in the range of $(0, 1)$. It should be noted that $\nabla^2\bar{\phi} = 0$ and $\partial\bar{\sigma}/\partial r = 1/\delta\sqrt{\pi}\exp(-(r - a)^2/\delta^2)$. In this paper, the range of δ is fixed, $\delta \in [0.05, 0.15]$. To verify (3.12), we assume that the concentration has a Heaviside profile initially, the conductivity profile at time instant t is solved numerically by the dimensionless form of (3.3) and a regular condition is imposed at the centreline $\mathrm{d}\sigma/\mathrm{d}r = 0$.

The base conductivity profile is shown in figure 2. It is obvious that the electrical conductivity profile can be approximated by the error function in (3.12) by adjusting the value of δ at an instant t. In the following study, we use (3.12) as the profile of the electrical conductivity at the base state for convenience in the study of linear stability.

4. Linear stability analysis

The linear stability analysis of the flow system is implemented by perturbing the base state with infinitesimal disturbances:

$$[u, v, w, p, \sigma, \phi] = [0, 0, \bar{w}, \bar{p}, \bar{\sigma}, \bar{\phi}] + [u', v', w', p', \sigma', \phi'], \tag{4.1}$$

where the primed variables are the infinitesimal disturbances. In a standard way, we consider the normal mode analysis:

$$[u', v', w', p', \sigma', \phi'] = [\hat{u}, \hat{v}, \hat{w}, \hat{p}, \hat{\sigma}, \hat{\phi}]\exp(\mathrm{i}(m\theta + \alpha z) + \lambda t), \tag{4.2}$$

in which $[\hat{u}, \hat{v}, \hat{w}, \hat{p}, \hat{\sigma}, \hat{\phi}]$ is the Fourier amplitude, m is the azimuthal wavenumber, α is the streamwise wavenumber and λ is the complex temporal growth rate.

On substituting (4.1) with the normal mode analysis into (3.5), (3.6), (3.8) and (3.9) and after linearizing, we obtain the governing equations of the eigenvalue problem:

$$D\hat{u} + \frac{\hat{u} + im\hat{v}}{r} + i\alpha\hat{w} = 0, \tag{4.3}$$

$$\lambda\hat{u} = -D\hat{p} - i\alpha\bar{w}\hat{u} + \frac{1}{Re}\left(\mathscr{L}\hat{u} - \frac{\hat{u} + 2im\hat{v}}{r^2}\right), \tag{4.4}$$

$$\lambda\hat{v} = -\frac{im\hat{p}}{r} - i\alpha\bar{w}\hat{v} + \frac{1}{Re}\left(\mathscr{L}\hat{v} - \frac{\hat{v} - 2im\hat{u}}{r^2}\right), \tag{4.5}$$

$$\lambda\hat{w} = -i\alpha\hat{p} - i\alpha\bar{w}\hat{w} - D\bar{w}\hat{u} + \frac{1}{Re}\mathscr{L}\hat{w} - \frac{Q}{PeRe}\mathscr{L}\hat{\phi}, \tag{4.6}$$

$$Pe\lambda\hat{\sigma} = -PeD\bar{\sigma}\hat{u} - iPe\alpha\bar{w}\hat{\sigma} + \mathscr{L}\hat{\sigma}, \tag{4.7}$$

$$[(\eta - 1)\bar{\sigma} + 1]\mathscr{L}\hat{\phi} + (\eta - 1)D\bar{\sigma}D\hat{\phi} - i\alpha(\eta - 1)\hat{\sigma} = 0, \tag{4.8}$$

where $\mathscr{L} = D^2 + (1/r)D - (m^2/r^2) - \alpha^2$, $D = d/dr$. The Péclet number $Pe = ReSc$. It should be noted that the value of Pe cannot be small because diffusion of conductivity is slow.

The boundary conditions at $r = 1$ are

$$\hat{u} = \hat{v} = \hat{w} = D\hat{\sigma} = D\hat{\phi} = 0. \tag{4.9}$$

At the centreline $r = 0$, the singular nature of the cylindrical coordinate system requires special treatment. To deal with the singular point of the system (4.3)–(4.8), we use the fact that the velocity vector and the other scalar variables have a vanishing azimuthal dependence as they approach the centreline, i.e.

$$\lim_{r=0}\frac{\partial \boldsymbol{v}'}{\partial\theta} = \lim_{r=0}\frac{\partial p'}{\partial\theta} = \lim_{r=0}\frac{\partial \sigma'}{\partial\theta} = \lim_{r=0}\frac{\partial \phi'}{\partial\theta} = 0, \tag{4.10}$$

where $\boldsymbol{v}' = u'\boldsymbol{e}_r + v'\boldsymbol{e}_\theta + w'\boldsymbol{e}_z$ is the velocity disturbance.

In the form of Fourier modes, the regular boundary conditions are

$$im\hat{u} - \hat{v} = \hat{u} + im\hat{v} = m\hat{w} = m\hat{p} = m\hat{\sigma} = m\hat{\phi} = 0. \tag{4.11}$$

If $m = 0$, the boundary conditions are

$$\hat{u} = \hat{v} = D\hat{w} = D\hat{p} = D\hat{\sigma} = D\hat{\phi} = 0. \tag{4.12}$$

If $m = 1$, the boundary conditions are

$$D\hat{u} = D\hat{v} = \hat{w} = \hat{p} = \hat{\sigma} = \hat{\phi} = 0. \tag{4.13}$$

The velocity conditions of $m = 1$ agree with the boundary conditions given by Khorrami (1991) for a single fluid flow in a circular pipe.

When $m \geqslant 2$, the boundary conditions are

$$\hat{u} = \hat{v} = \hat{w} = \hat{p} = \hat{\sigma} = \hat{\phi} = 0. \tag{4.14}$$

A Chebyshev collocation method is implemented to solve the eigenvalue problem, and the physical domain is transformed into the Chebyshev domain,

$$\zeta = 2r - 1. \tag{4.15}$$

The variables $\hat{u}$, $\hat{v}$, $\hat{w}$, $\hat{p}$, $\hat{\sigma}$, $\hat{\phi}$ are expanded as

$$\hat{u} = \sum_0^N a_n T_n(\zeta), \quad \hat{v} = \sum_0^N b_n T_n(\zeta), \quad \hat{w} = \sum_0^N c_n T_n(\zeta), \qquad (4.16a\text{--}c)$$

$$\hat{p} = \sum_0^N d_n T_n(\zeta), \quad \hat{\sigma} = \sum_0^N f_n T_n(\zeta), \quad \hat{\phi} = \sum_0^N e_n T_n(\zeta), \qquad (4.17a\text{--}c)$$

where $T_n(\zeta)$ denotes the nth Chebyshev polynomial.

In order to modify the computation near the interface $r = a$, the Chebyshev collocation points are clustered in the mixing region at $r = a$ using the following stretching function (Govindarajan 2004):

$$\xi = \frac{a}{\sinh(f_b r_0)}[\sinh[(r - r_0)] + \sinh(f_b a)], \qquad (4.18)$$

where $r_0 = 1/2f_b \ln[(1 + (\exp(f_b - 1)a)/1 + (\exp(-f_b) - 1)a)]$. The coefficient f_b determines the degree of clustering, and $f_b = 6$ in this paper. The parameter a represents the location of the interface around which clustering is desired.

After clustering the Chebyshev collocation points into the diffusion region, we need to calculate the eigenvalue problem via the clustered grid. Therefore, a transformation on the derivatives between the clustered grid and the Chebyshev grid should be made,

$$\frac{\mathrm{d}f}{\mathrm{d}\xi} = \frac{\mathrm{d}f}{\mathrm{d}r}\frac{\mathrm{d}r}{\mathrm{d}\xi} = \frac{1}{G'(r)}\frac{\mathrm{d}f}{\mathrm{d}r}, \qquad (4.19)$$

where $G(r) = \xi$ and f stands for the variable $\hat{u}$, $\hat{v}$, $\hat{w}$, $\hat{p}$, $\hat{\sigma}$ or $\hat{\phi}$. It should be noted that the derivative $\mathrm{d}f/\mathrm{d}r = 2(\mathrm{d}f/\mathrm{d}\zeta)$.

For the second derivative of f, using the chain rule, the transformation is written

$$\frac{\mathrm{d}^2 f}{\mathrm{d}\xi^2} = \frac{1}{(G')^2}\frac{\mathrm{d}^2 f}{\mathrm{d}r^2} - \frac{G''}{(G')^3}\frac{\mathrm{d}f}{\mathrm{d}r}. \qquad (4.20)$$

The derivative $\mathrm{d}^2 f/\mathrm{d}r^2 = 4(\mathrm{d}^2 f/\mathrm{d}\zeta^2)$. Numerical validation of our method will be made in the following discussion.

5. Energy analysis

In order to understand the physical mechanism, we apply the energy analysis (Govindarajan, L'vov & Procaccia 2001). We multiply the conjugates of the variables $\hat{u}^*$, $\hat{v}^*$ $\hat{w}^*$ on both sides of (4.4)–(4.6). The real part of the equation obtained by summing these equations and integrating over the cross-sectional area gives the energy balance:

$$\dot{E}_k = I + V + E_e. \qquad (5.1)$$

Here, the kinetic energy growth rate is

$$\dot{E}_k = \lambda_r \int_0^1 r(|\hat{u}|^2 + |\hat{v}|^2 + |\hat{w}|^2)\mathrm{d}r, \qquad (5.2)$$

	$c\,(m=0,\ \alpha=1)$	$c\,(m=1,\ \alpha=0.5)$	$\lambda'\,(m=1,\ \alpha=0)$
SH	$0.93675536-0.06374551\mathrm{i}$	$0.84646970-0.07176332\mathrm{i}$	-0.00734099
Present work	$0.93675536-0.06374551\mathrm{i}$	$0.846469697-0.07176332\mathrm{i}$	-0.007340985

TABLE 1. The first leading eigenvalues of the system for $Re=2000$, $Pe=Q=0$. We have utilized 51 points for the eigenvalue problem and related the eigenvalues to those of SH by defining $\lambda'=\mathrm{i}\lambda$ and $c=\lambda'/\alpha$.

the work done by the Reynolds stress is

$$I = -\int_0^1 r\,\mathrm{Re}(\mathrm{D}\bar{w}\hat{w}^*\hat{u})\,\mathrm{d}r \qquad (5.3)$$

and the viscous dissipation is

$$V = -\frac{1}{Re}\int_0^1 r\left\{(|\mathrm{D}\hat{u}|^2+|\mathrm{D}\hat{v}|^2+|\mathrm{D}\hat{w}|^2)+\left(\frac{m^2}{r^2}+\alpha^2\right)(|\hat{u}|^2+|\hat{v}|^2+|\hat{w}|^2)\right.$$
$$\left.+\frac{|\hat{u}|^2+|\hat{v}|^2}{r^2}-4m\frac{\mathrm{Im}(\hat{u}^*\hat{v})}{r^2}\right\}\mathrm{d}r. \qquad (5.4)$$

The work done by the electrical force is

$$E_e = \frac{Q}{PeRe}\int_0^1 r\mathrm{Re}\left(\mathrm{D}\hat{w}^*\mathrm{D}\hat{\phi}+\frac{m^2\hat{w}^*\phi}{r^2}+\alpha^2\hat{w}^*\phi\right)\mathrm{d}r. \qquad (5.5)$$

Since the magnitude of the eigenfunction is arbitrary, we normalize the eigenfunction by its maximum absolute value. The terms in the energy analysis are rescaled with respect to the total kinetic energy $\int_0^1 r(|\hat{u}|^2+|\hat{v}|^2+|\hat{w}|^2)\,\mathrm{d}r$. For an unstable flow, $\dot{E}$ should be positive. The energy analysis will be applied to interpret the instability mechanism in the following discussion.

6. Results and discussion

6.1. *Validation of numerical methods*

We examine the validation of our numerical method by setting $Q=Pe=0$; therefore, the electric field is turned off and ionic advection is absent. Since we are setting $Q=0$ and (4.8) does not produce any eigenvalues, the conductivity profile has no influence on the spectrum of the problem and the eigenvalue problem should be identical to a single fluid flowing in a circular pipe. We compare our numerical results with those of Schmid & Henningson (2001) (hereafter referred to as SH) for $Re=2000$. The leading eigenvalue is listed in table 1. Excellent agreement between our numerical results and those of SH demonstrates the validity of our numerical method.

It should be noted that, when $Re\to 0$, i.e. the inertia of the fluid is negligible, the growth rate is determined by the ionic diffusion equation (4.7). In a viscosity stratified plane-Poiseuille flow (Talon & Meiburg 2011), the eigenspectrum of the diffusion equation presents a similar structure to the Orr–Sommerfeld problem. Hence, the diffusion equation will produce more eigenvalues in the stratified flow than a single fluid flow (Talon & Meiburg 2011). Similarly, in pipe flow with conductivity
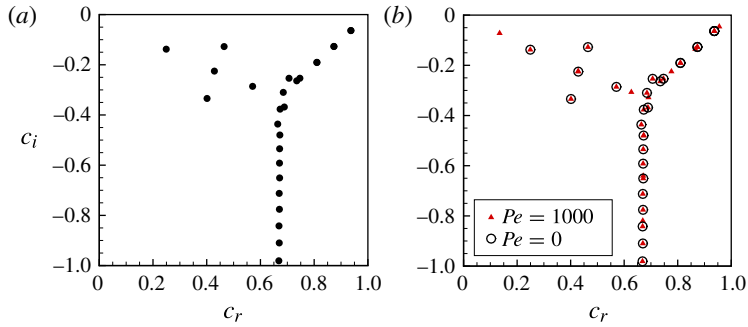
FIGURE 3. (Colour online) Eigenspectra for $Re = 2000$, $m = 0$, $\alpha = 1$. (*a*) The eigenspectrum for Hagen–Poiseuille flow which is identical to that of SH. (*b*) A comparison of conductivity stratified pipe flow (triangular points) and Hagen–Poiseuille flow (circles). The conductivity ratio $\eta = 2$ and the parameters are $Q = 0$, $a = 0.5$, $\delta = 0.05$. It is obvious that when $Pe > 0$, there are some extra eigenvalues compared with Hagen–Poiseuille flow. The parameter $c = i\lambda/\alpha$.

stratification, the eigenspectrum structure will be different from the result of SH, as demonstrated in figure 3. In the following discussion, we consider that the base flow in the pipe is weak and focus on the instability caused by the electrical force in microfluidic channels.

6.2. *Parametric study*

6.2.1. *Effect of the conductivity ratio*

The influence of the conductivity ratio on the linear stability analysis is of particular interest and will be investigated in this section. Before presenting the numerical study, let us consider the case of two liquids with the same electrical conductivity, i.e. $\eta = 1$. The linearized electrical current conservation (4.8) reduces to

$$\mathscr{L}\hat{\phi} = 0. \tag{6.1}$$

Hence, in the linearized momentum equation (4.6), the electrical force that can trigger instability is absent. Therefore, the system will be linearly stable. Numerical study also indicates that the eigenvalue λ is not influenced by the electrical number Q for $\eta = 1$ and $\lambda_r < 0$ (see table 3 in appendix A). We can obtain a useful result here: the system becomes more stable as η increases when $\eta < 1$, while the system becomes more unstable as η increases when $\eta > 1$. To study the influence of the conductivity ratio on the linear stability, the other parameters are fixed: $Re = 1$, $Sc = 1000$, $a = 0.5$ and $\delta = 0.1$. To study the linear stability problem, 51 collocation points are sufficient to provide satisfying accuracy.

First, we consider two typical cases: $\eta = 0.5$, $\eta = 2$. The electrical number Q is fixed so as to study the growth rate of the disturbance. The results in figure 4(*a*) demonstrate that the azimuthal disturbances make the system more unstable. They also imply that the azimuthal wavenumber m of the critical mode is $m = 1$. The results are different in figure 4(*b*). They show that the azimuthal wavenumber of the most unstable mode is $m = 0$ for $\eta = 2$. These results imply that the critical unstable mode of the system varies with the conductivity ratio η. To elucidate the critical unstable mode in the system, we investigate the marginal curves in the Q–α plane. Figure 5
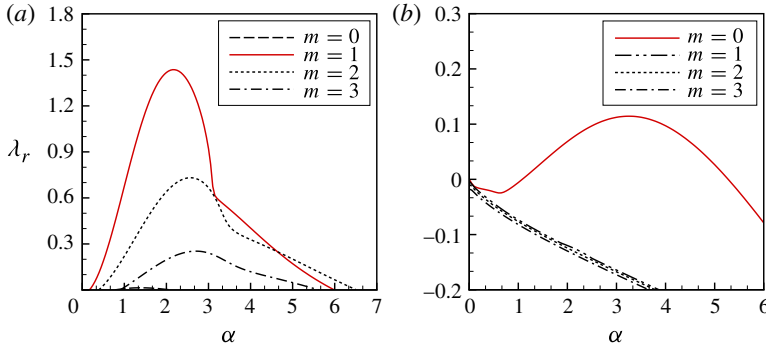
FIGURE 4. (Colour online) The real temporal growth rate λ_r versus the wavenumber α:
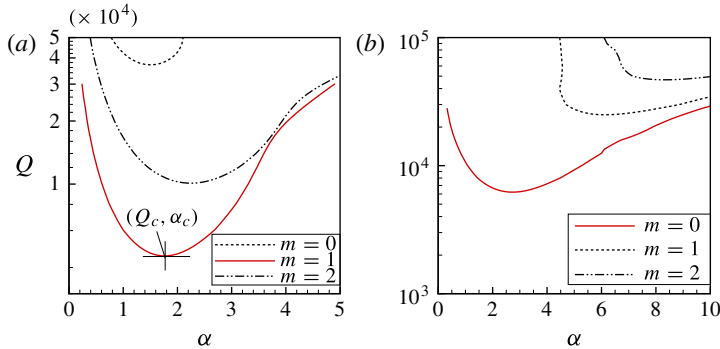(*a*) $Q = 5 \times 10^4$, $\eta = 0.5$; (*b*) $Q = 10^4$, $\eta = 2$.

FIGURE 5. (Colour online) The marginal stability curves: (*a*) $\eta = 0.5$; (*b*) $\eta = 2$.

demonstrates that the wavenumber m of the critical unstable mode for $\eta = 0.5, 2$ is $m = 1, 0$ respectively. The azimuthal wavenumber of the critical unstable mode is defined as the critical azimuthal wavenumber m_c. Here, we define Q_c as the critical electrical number and α_c as the critical streamwise wavenumber. We have examined the eigenvalue λ of the critical unstable modes in figure 5 whose imaginary part is non-zero. It indicates that the critical unstable modes are oscillatory. The perturbed fields of the charge density and the conductivity in the r–θ plane are shown in figure 6 to illustrate the two different unstable modes. In figure 6(*a*,*b*), the unstable mode is defined as the corkscrew mode, while the unstable mode in 6(*c*,*d*) is defined as the axisymmetric mode. We numerically evaluate the energy contribution of E_e which is always positive. It demonstrates that the electrical force is the main factor that destabilizes the system. The instability is referred to as the dielectrophoretic instability (Baygents & Baldessari 1998; Chang *et al.* 2009; Ding & Wong 2014).

In order to reveal the influence of the conductivity ratio on the critical unstable mode, i.e. in what range of η the critical unstable mode is the corkscrew mode or the axisymmetric mode, we investigate the behaviour of (Q_c, m_c, c) versus the value of η. The wave speed c of the critical mode is defined as

$$c = -\lambda_i / \alpha_c. \qquad (6.2)$$

The results in figure 7(*a*) indicate that the system becomes more unstable for a larger contrast in the electrical conductivity between the two layers. A similar
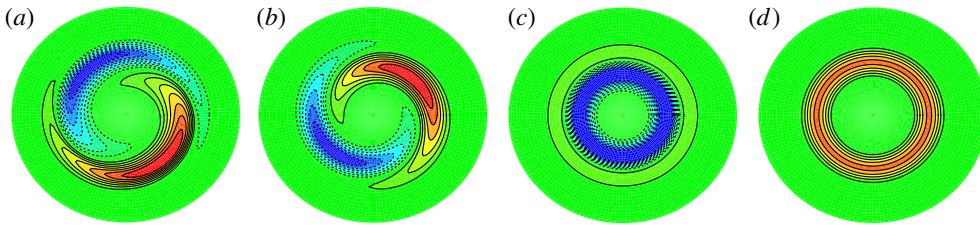
FIGURE 6. (Colour online) (*a,b*) The perturbed field of the electrical charge ρ_e and the perturbed field of the conductivity σ for $\eta = 0.5$, $Q_c = 4505.8$, $m_c = 1$, $\alpha_c = 1.75$ in the r–θ plane. (*c,d*) The perturbed field of the electrical charge ρ_e and the perturbed field of the conductivity σ for $\eta = 2$, $Q_c = 6197.0$, $m_c = 0$, $\alpha_c = 2.75$ in the r–θ plane.

phenomenon has been observed by Lin *et al.* (2004) in a liquid layer with conductivity stratification in a square channel. Experimental observation and stability analysis suggested that the flow became more unstable for a larger conductivity contrast (Lin *et al.* 2004). However, they focused on the two-dimensional instability, and the way in which the conductivity ratio influenced the three-dimensional stability was not investigated (Lin *et al.* 2004). In this paper, we investigate the three-dimensional instability and our results in figure 7(*c*) show that the critical wavenumber m_c jumps from 1 to 0 as the conductivity ratio increases to $\eta = 1$. This figure indicates that, for the selected input values of other dimensionless parameters, the critical unstable mode is dominated by the corkscrew mode when the inner conductivity is larger, while the axisymmetric mode dominates the instability when the outer conductivity is larger. Moreover, in a square-duct flow system, Lin *et al.* (2004) gave the physical properties of the flow system for a conductivity ratio $\eta = 10$, which are applied to estimate the critical strength of the applied electric field in our present system. Our results show that, for $\eta = 10$, the critical value electrical number $Q_c \approx 10^3$. This gives the critical electrical strength $E \approx 2 \times 10^3$ V m^{-1} provided that the electrical permittivity $\epsilon = 6.9 \times 10^{-10}$ C V^{-1} m^{-1}, the dynamic viscosity $\mu = 10^{-3}$ kg m^{-1} s^{-1}, the effective diffusivity $K_{eff} = 2 \times 10^{-9}$ m^2 s^{-1} and the pipe radius $b = 10^{-3}$ m. Hence, it is possible to achieve electromixing in a circular pipe at small Reynolds flow by an electric field in experiments. Figure 7(*b*) shows that $\lambda_i \neq 0$, which demonstrates that the unstable mode is oscillatory. Figure 7(*d*) shows that the critical wave speed c increases with increasing η. Figure 7(*d*) also shows that, when $\eta < 1$, the wave speed is smaller for a larger conductivity contrast; when $\eta > 1$, the wave speed is larger for a larger conductivity contrast. Additionally, the wave speed $c > 0$ indicates that the linear wave propagates downstream.

6.2.2. *Effect of interface location*

This section discusses the influence of the interface location on the linear stability of the system. The other parameters are fixed at $Re = 1$, $Sc = 1000$, $\delta = 0.05$ so as to investigate the dielectrophoretic instability. Here, $\delta = 0.05$ is chosen under the consideration of a sharper interface. Two conductivity ratios $\eta = 0.5, 2$ will be considered in the following discussion. We examined the convergence of our numerical method and found that $N = 60$ is sufficient to provide adequate resolution at reasonable computational cost.

Selvam *et al.* (2007) found that the interface location had a significant influence on the critical instability of a viscosity stratified pipe flow and the least unstable mode
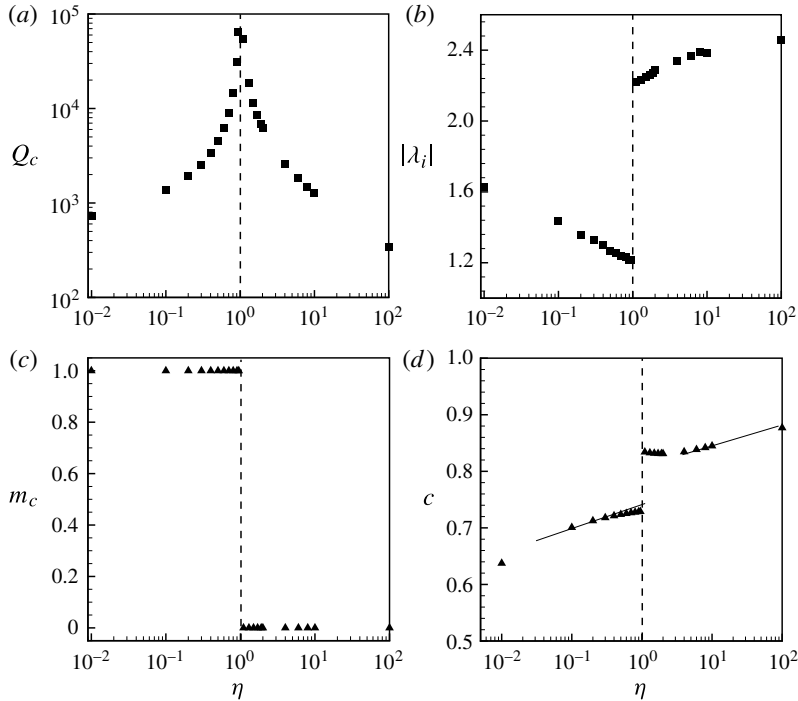
FIGURE 7. (*a*) The critical electrical strength number Q_c versus η; (*b*) the critical frequency $|\lambda_i|$ versus η; (*c*) the critical wavenumber m_c versus η; (*d*) the wave speed of the critical mode c versus η.

occurred at approximately 0.6 times the pipe radius. In our problem of a liquid with conductivity stratification, a similar phenomenon is observed. However, the instability of our problem is triggered by the electric field, while in the problem studied by Selvam *et al.* (2007), the instability is due to the Reynolds stress. If the interfacial location is very near the centreline or the pipe wall, the diffusion of ions will rapidly remove the conductivity difference. Furthermore, we consider a very sharp interface, when $a \to 0$ or $a \to 1$, so no matter how large an electric field is imposed, the system should be stable due to the homogenous conductivity profile. Hence, it can be concluded that, as the interface is slightly moved away from the centreline, the system becomes more unstable. As the interface approaches the outer boundary, the system should become more stable. Therefore, there should be an optimal location of the interface where the flow is least stable. Two typical cases of $\eta = 0.5, 2$ have been investigated numerically and the range of the interface location a is considered to be in [0.1, 0.9]. The variation of the critical wavenumber m_c and the critical electrical number Q_c with the location a is shown in figure 8. Figure 8(*a*) demonstrates that, for $\eta = 0.5, 2$, the system becomes more unstable as a increases from 0.1 until $a \approx 0.3$, $a \approx 0.2$ respectively, while it becomes more stable as a increases further. Additionally, for $\eta = 0.5$, we observe that the critical unstable mode shifts from the corkscrew mode $m_c = 1$ to the axisymmetric mode $m_c = 0$ as a increases to a critical value $a \approx 0.83$. For $\eta = 2$, the axisymmetric mode dominates the instability.

We are interested in the maximum growth rate of the system since the rapid mixing is of particular interest (Lin *et al.* 2004). To investigate the maximum growth rate,
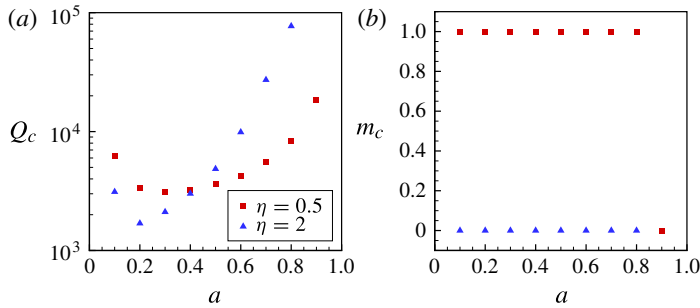
FIGURE 8. (Colour online) (*a*) The critical electrical strength number Q_c versus a; (*b*) the critical wavenumber m_c versus a.
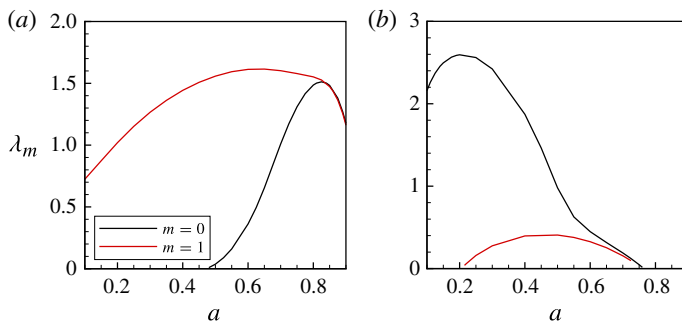

FIGURE 9. (Colour online) The maximum growth rate λ_m versus a: (*a*) $Q = 5 \times 10^4$, $\eta = 0.5$; (*b*) $Q = 5 \times 10^4$, $\eta = 2$.

the electrical number is fixed. We examine the behaviour of the maximum growth rate $\lambda_m = \max(\text{Re}(\lambda))$ versus the interface location a. The maximum growth rate λ_m describes the growth rate of the most unstable mode. The corkscrew mode and the axisymmetric mode are investigated, as shown in figure 9. Figure 9(*a*) shows that the maximum growth rate occurs at $a \approx 0.6$. We examined the maximum growth rate λ_m versus a by reducing the value of Q and found that the peak point in the λ_m–a plane moved leftwards, as shown in figure 10(*a*). This implies that, for a strong electric field, the most unstable mode prefers an intermediate a for $\eta = 0.5$ although the critical unstable mode prefers $a \approx 0.3$. The mechanism is very complex because the electrical force destabilizes the flow while the viscous dissipation and the ionic diffusion tend to stabilize the system. In order to explain the results, we apply the energy analysis. As the interface location a increases, the viscous dissipation effect becomes weaker until $a \approx 0.6$, after which it becomes stronger as a increases further, as shown in figure 10(*b*). This is the reason why for an unstable flow, $Q = 5 \times 10^4$, the maximum growth rate occurs at $a \approx 0.6$. In addition, we observe that, for $\eta = 0.5$, the maximum growth rate of the axisymmetric mode dominates the corkscrew mode when $a \gtrsim 0.83$ for $Q = 5 \times 10^4$. This indicates that the axisymmetric mode becomes critical when the interface approaches the pipe wall. Figure 9(*b*) demonstrates that the maximum growth rate occurs at $a \approx 0.2$, which indicates that the most unstable mode and the critical unstable mode prefer $a \approx 0.2$. Additionally, it is observed that, for $\eta = 2$, the axisymmetric mode always dominates the corkscrew mode.
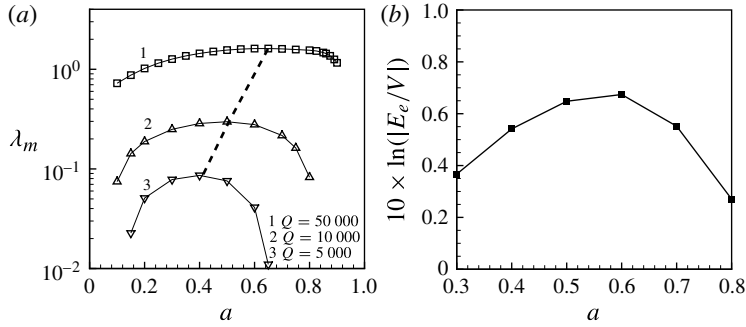
FIGURE 10. (*a*) The maximum growth rate λ_m of the corkscrew mode $m = 1$ versus *a* for different values of the input electrical number *Q*. (*b*) The log ratio between the energy E_e and *V*, in which the electrical number $Q = 5 \times 10^4$ and the wavenumber α corresponds to the most unstable mode.
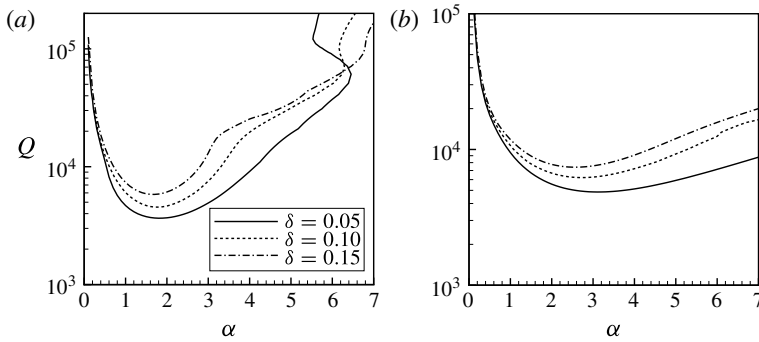

FIGURE 11. The marginal stability curves: (*a*) $\eta = 0.5$; (*b*) $\eta = 2$.

6.2.3. *Effect of interface thickness*

This section investigates of the influence of the interface thickness on the critical instability. The other parameters are fixed: $Re = 1$, $Sc = 1000$, $a = 0.5$. In the above discussion, we have considered two values of δ. It is observed that the system becomes more stable for a larger value of δ. The marginal stable curves for three typical values of δ are shown in figure 11. For a liquid with viscosity stratification, Selvam *et al.* (2007) reported that, for a thicker interface, the flow became more stable. Selvam *et al.* (2007) explained that the stabilizing effect was due to the diffusion effect becoming more significant for a thicker interface, which dissipated the kinetic energy and inhibited the instability. Two studies by Chang *et al.* (2009) and Ding & Wong (2014) show that the system becomes more stable with reduction of the conductivity gradient when the conductivity gradient is small, while the flow becomes more stable as the conductivity gradient increases when the conductivity gradient is large. In our present study, if we fix the conductivity ratio, the conductivity gradient within the interface becomes smaller as the interface becomes thicker. Our study shows that the flow becomes more stable as the conductivity gradient decreases, which is different from the previous two studies by Chang *et al.* (2009) and Ding & Wong (2014). In fact, in our current study, a thicker interface implies that the system undergoes a longer diffusion time. Assuming that the conductivity is uniform
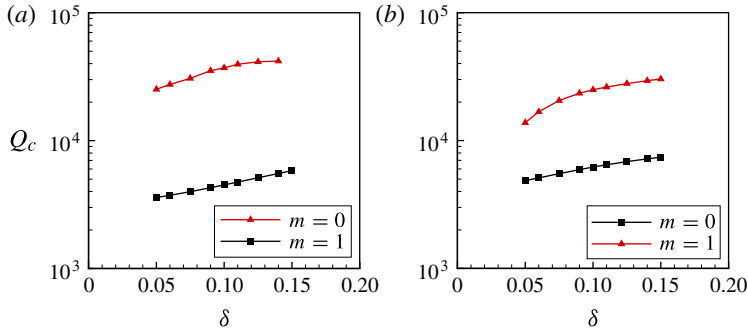
FIGURE 12. (Colour online) The critical electrical strength number Q_c versus δ: (a) $\eta = 0.5$; (b) $\eta = 2$.

in the system due to diffusion for quite a long time, we would expect a completely stable flow. Therefore, the system may become more stable as the interface becomes thicker. Numerical studies demonstrate that, with increasing interface thickness δ, the marginal curve rises up in the Q–α plane, which indicates that the flow becomes more stable as the interface becomes thicker, supporting our analysis. Our result is similar to the phenomenon in a viscosity stratified flow (Selvam *et al.* 2007), but different from the studies by Chang *et al.* (2009) and Ding & Wong (2014). The difference is due to the fact that the flow studied by Chang *et al.* (2009) and Ding & Wong (2014) is bounded by two solid walls. However, in our problem, the flow is only bounded by the outer pipe wall. We observe that, for the axisymmetric mode, $\eta = 2$, the critical wavenumber α_c becomes smaller as δ increases, as seen in figure 11(b). This indicates that the wavelength of the disturbance becomes longer as δ increases. In order to show the effect of δ on the critical stability, the critical electrical number Q_c is plotted against δ in figure 12. Figure 12 also demonstrates that the system becomes more stable as δ increases. Additionally, the corkscrew mode dominates the instability for $\eta = 0.5$, and the axisymmetric mode dominates the instability for $\eta = 2$.

6.2.4. *Effect of shear flow*

In this section, we aim to reveal the influence of the shear flow on the dielectrophoretic instability. The other parameters are fixed at $a = 0.5$, $\delta = 0.1$. Before presenting the numerical study, let us consider the electrical force term in the linearized axial momentum equation (4.6):

$$-\frac{Q}{RePe}\mathscr{L}\hat{\phi} = \frac{Q}{Re^2Sc}\hat{\rho}_e. \qquad (6.3)$$

The value of Sc is fixed at $Sc = 1000$. Equating $Q/(Re^2Sc)$ at two different values of Re gives

$$Q_2 = \frac{Re_2^2}{Re_1^2}Q_1. \qquad (6.4)$$

This relation reflects the fact that, when the value of $Q/(Re^2Sc)$ is fixed, a smaller Re describes a smaller Q. This implies that, when the Reynolds number is small, the system may be more unstable. In this paper, we consider a weak shear flow under the consideration of flow in a microfluidic channel and propose that Re has a range
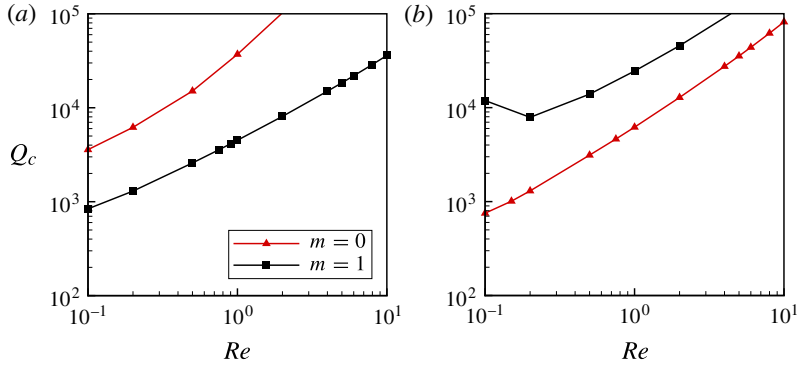
FIGURE 13. (Colour online) The critical electrical strength number Q_c versus Re: (a) $\eta = 0.5$; (b) $\eta = 2$.

of $[0.1, 10]$ provided that the pipe radius is 10^{-3} m and the kinematic viscosity $\nu = 10^{-6}$ m^2 s^{-1}. The maximum velocity occurring at the centreline $r = 0$ can be varied from 10^{-4} to 10^{-2} m s^{-1}.

It is observed that, for $\eta = 0.5$, the corkscrew mode dominates the instability, and for $\eta = 2$, the axisymmetric mode dominates the instability. Figure 13 illustrates that the critical electrical number Q_c increases as Re increases, indicating that the shear flow impedes the electro-convection in the system. Interestingly, the corkscrew mode for $\eta = 2$ can be enhanced by the shear flow, as seen in figure 13(b), although it never becomes critical for the selected input values of Re, η and Sc. It is different from the previous studies by Chang *et al.* (2009) and Ding & Wong (2014), which show that the critical instability can be either enhanced or impeded by the shear flow. In the present study, we observe that the shear flow always impedes the critical instability. In order to understand the physical mechanism, we fix the value of Q and the wavenumber α to investigate the energy contributions of the electrical force, Reynolds stress and viscous stress. For some Re, the flow is stable, e.g. $Re > 2.5$ for $\eta = 0.5$ and $Re > 2$ for $\eta = 2$. The electrical energy becomes smaller, as demonstrated in figure 14(a). We have found that $\dot{E}_k$ becomes smaller as Re increases and becomes negative as Re exceeds some critical value, which indicates that the system becomes stable as Re increases. However, the underlying factor that stabilizes the system is not the reduction in the electrical energy. Figure 14(b) shows that, as the Reynolds number increases, $\ln(|E_e/V|)$ decreases for $\eta = 0.5$, while $\ln(|E_e/V|)$ increases for $\eta = 2$. This indicates that the stabilizing mechanisms in the two cases $\eta = 0.5, 2$ are different. We have examined the case of $Re = 10$ and found that, for $\eta = 0.5$, $\ln(|E_e/V|) < 0$, while for $\eta = 2$, $\ln(|E_e/V|) > 0$. This indicates that, for $\eta = 0.5$, the increase of the viscous dissipation is the major factor that stabilizes the flow, although the Reynolds stress also plays a stabilizing role, as shown in figure 14(c). For $\eta = 2$, because the electrical energy always dominates the viscous dissipation, i.e. $E_e > |V|$, the stabilizing factor in the system is due to the Reynolds stress, which dissipates the kinetic energy of the perturbation. The results indicate that the imposed shear flow can impede the dielectrophoretic instability via the dissipation mechanisms of the viscous stress and the Reynolds stress.

Furthermore, we investigated the influence of Re on the wave speed c. Results are shown in figure 15. It is observed that, for $\eta = 0.5$, the critical wave speed c increases slightly as Re increases initially, then it has a negligible influence on the wave speed.
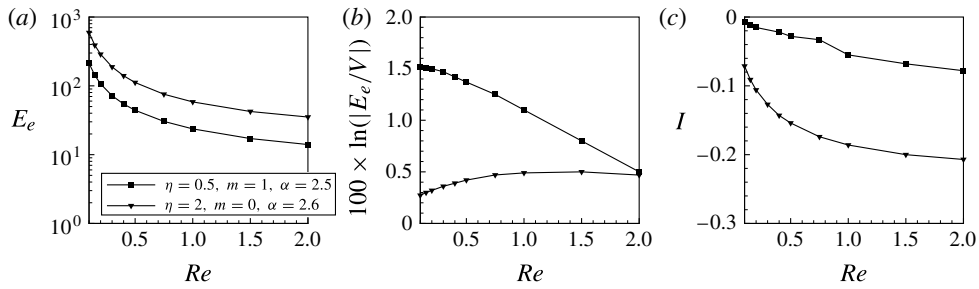
FIGURE 14. (*a*) Electrical energy E_e versus Re; (*b*) the log ratio between the electrical energy and the viscous dissipation versus Re; (*c*) the work of the Reynolds stress versus Re. The electrical number $Q = 10^4$.
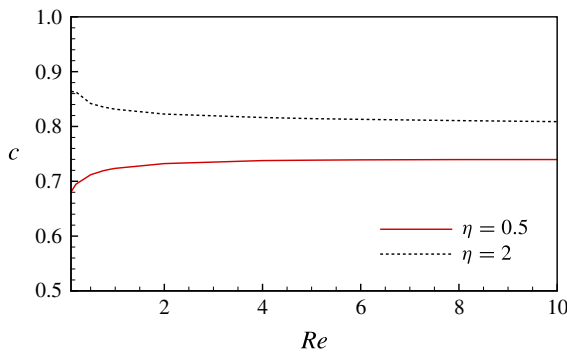

FIGURE 15. (Colour online) The wave speed of the critical unstable mode versus the Reynolds number.

However, the wave speed decreases slightly as Re increases from $Re = 1$ for $\eta = 2$, and then the wave speed seems to be independent of Re. The results by Chang *et al.* (2009) indicated that the critical frequency of the critical transverse unstable mode $-\lambda_i$ was independent of the Reynolds number when $Re > 1$. This implies that the critical wave speed is independent of Re. In our system, we observe that the wave speed c is independent of Re for both the two critical unstable modes, the corkscrew mode and the axisymmetric mode, when $Re > 2$.

6.2.5. *Effect of ionic diffusion*

This section presents a study of the influence of the ionic diffusion on the dielectrophoretic instability. The other parameters are fixed: $Re = 1$, $a = 0.5$, $\delta = 0.1$. In the governing equations (4.3)–(4.8), replacing Re by Pe does not change the governing equations, which indicates that the effect of ionic diffusion on the flow instability should be similar to that of Re. However, the results should not be the same as shown in § 6.2.4 above, in which Re is varied while Sc is fixed. Therefore, it is necessary to investigate the influence of Sc on the stability by fixing the value of Re.

The critical electrical number Q_c versus the Schmidt number is shown in figure 16. The corkscrew mode dominates the instability for $\eta = 0.5$ and the axisymmetric mode dominates the instability for $\eta = 2$, as shown in figure 16. The system becomes
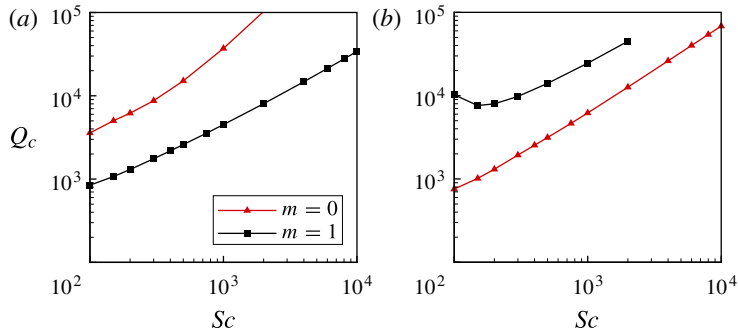
FIGURE 16. (Colour online) The critical electrical strength number Q_c versus Sc: (*a*) $\eta = 0.5$; (*b*) $\eta = 2$.

more stable as Sc increases. The results in figure 16 are quite similar to those in figure 13, which demonstrates that the influence of Sc on the flow stability is similar to that of Re.

The instability mechanism is then interpreted by the energy analysis. We consider the critical instability of the system when $\dot{E}_k = 0$. The viscous dissipation term V is always negative and plays a stabilizing role. The electrical force work $E_e > 0$, which triggers the electro-convection in the system. We calculated $\ln(|E_e/V|)$ and found that its value increased with Sc initially, then it decreased as Sc increased further, as shown in figure 17(*a*). This indicates that the viscous dissipation effect becomes weaker as Sc increases from $Sc = 100$, while it becomes stronger when Sc is very large. When Sc is not too large, $Sc = O(10^2)$, the Reynolds stress plays a key role in stabilizing the system since its dissipation effect becomes stronger as Sc increases, as shown in figure 17(*b*). As Sc increases further, for $\eta = 0.5$, the dissipation effect by the Reynolds stress becomes weaker, while for $\eta = 2$, the work of the Reynolds stress reaches a plateau, as seen in 17(*b*). Such a phenomenon indicates that, although the Reynolds stress dissipates the kinetic energy, it is not the major factor that causes the system to be more stable when we increase Sc. As shown in figure 17(*a*), $\ln(|E_e/V|)$ starts to decrease when Sc exceeds a certain value. This indicates that the viscous dissipation increases with Sc and becomes the major stabilizing factor. Moreover, we recall the definition of $Sc = \nu/K_{eff}$. This indicates that the viscous effect becomes stronger as the parameter Sc increases. Since viscous dissipation plays a stabilizing role, the system becomes more stable as Sc increases. The effect of Sc on the critical stability in this system is different from that in the previous studies by Chang *et al.* (2009) and Ding & Wong (2014). In these studies (Chang *et al.* 2009; Ding & Wong 2014), Sc was found to have a dual effect: increasing Sc can either enhance or inhibit the critical instability. Our study shows that, for $\eta = 2$, the corkscrew mode can be either enhanced or impeded as Sc increases, as seen in 16(*b*). However, the critical unstable mode always becomes stable. For an unstable flow, we observed that Sc can play a dual role in the system, in that the growth rate of disturbances can become either larger or smaller as Sc increases; this is not shown here since we are only interested in the critical stability of this system.

7. Conclusion

This paper investigated the electrodynamical instability of two miscible flows in a micro-pipe with electrical conductivity stratification. An axial electric field was
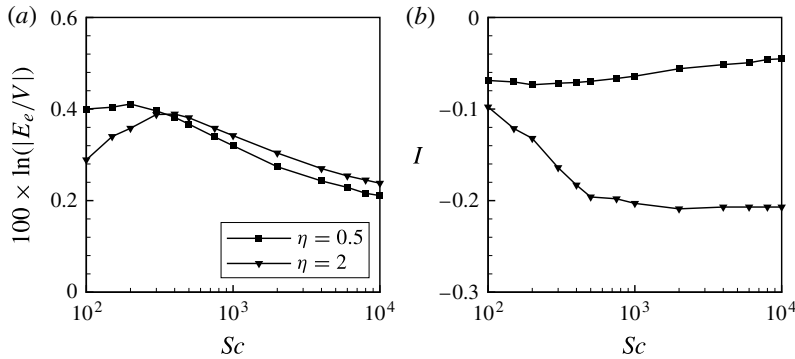
FIGURE 17. (*a*) The log ratio between the electrical energy and the viscous dissipation versus *Sc*; (*b*) the work of the Reynolds stress versus *Sc*.

	$N = 40$	$N = 50$	$N = 60$
λ	$0.291796693 - 1.449416017i$	$0.291796697 - 1.449416018i$	$0.291796697 - 1.449416018i$

TABLE 2. The first leading eigenvalues of the system for $Re = 1$, $Q = 10^4$, $Sc = 10^3$, $\eta = 0.5$, $a = 0.5$, $\delta = 0.05$, $\alpha = 2$, $m = 1$. This shows that our numerical method converges quickly by clustering the Chebyshev collocation points into the interfacial region.

imposed, which can trigger electro-convection in the system. A weak shear flow arose from an axial pressure gradient. A three-dimensional linear stability analysis was implemented to discuss the influences of conductivity ratio, interface location, interface thickness, shear flow and ionic diffusion on the critical stability of the flow. An energy analysis was carried out to interpret the instability mechanism.

It was found that the system was more unstable for a larger electrical conductivity contrast. When the electrical conductivity was larger within the inner layer, the critical unstable mode could be either the corkscrew mode or the axisymmetric mode, depending on the interface location. A detailed study showed that the critical unstable mode shifted from the corkscrew mode to the axisymmetric mode as the interface approached the pipe wall. When the electrical conductivity was larger in the outer layer, the critical unstable mode was dominated by the axisymmetric mode. The interface location had a significant influence on the critical unstable mode. The system was more stable when the interface was close to the centreline or the pipe wall. The flow became more stable as the interface became thicker, and the shear flow and ionic diffusion were found to have a stabilizing effect via the dissipation mechanisms of the Reynolds stress and viscous stress.

Acknowledgements

Appendix A

The general eigenvalue problem is denoted as

$$\mathscr{A}\boldsymbol{q} = \lambda \mathscr{B}\boldsymbol{q}, \tag{A 1}$$

	$Q' = 10$	$Q' = 100$	$Q' = 1000$
$c = i\lambda/\alpha$	$0.846469697 - 0.071763323i$	$0.846469697 - 0.071763323i$	$0.846469695 - 0.071763321i$

TABLE 3. The first leading eigenvalues of the system for $Re = 2000$, $Pe = 0$, $\alpha = 0.5$, $m = 1$, $\eta = 1$. We have also considered some other values of Re and the result shows that the eigenvalue is only dependent on Re. Changing the value of $Q' = (\epsilon E^2/\rho W^2)$ does not affect the eigenvalue for $\eta = 1$. The parameter Q' measures the ratio of electrical force to the fluid inertia.

where $\boldsymbol{q} = (\hat{u}, \hat{v}, \hat{w}, \hat{p}, \hat{\phi}, \hat{\sigma})^{\mathrm{T}}$ and

$$
\mathscr{A} = \begin{pmatrix}
D + \dfrac{1}{r} & \dfrac{im}{r} & i\alpha & 0 & 0 & 0 \\
L_1 & -\dfrac{2im}{Rer^2} & 0 & -D & 0 & 0 \\
\dfrac{2im}{Rer^2} & L_2 & 0 & -\dfrac{im}{r} & 0 & 0 \\
-D\bar{w} & 0 & L_3 & -i\alpha & L_4 & 0 \\
-PeD\bar{\sigma} & 0 & 0 & 0 & 0 & L_5 \\
0 & 0 & 0 & 0 & L_6 & -i\alpha(\eta - 1)
\end{pmatrix}, \qquad (A\,2)
$$

$$
\mathscr{B} = \begin{pmatrix}
0 & 0 & 0 & 0 & 0 & 0 \\
1 & 0 & 0 & 0 & 0 & 0 \\
0 & 1 & 0 & 0 & 0 & 0 \\
0 & 0 & 1 & 0 & 0 & 0 \\
0 & 0 & 0 & 0 & 0 & Pe \\
0 & 0 & 0 & 0 & 0 & 0
\end{pmatrix}, \qquad (A\,3)
$$

in which $L_1 = L_2 = 1/Re(\mathscr{L} - 1/r^2) - i\alpha\bar{w}$, $L_3 = (1/Re)\mathscr{L} - i\alpha\bar{w}$, $L_4 = -Q/(RePe)\mathscr{L}$, $L_5 = \mathscr{L} - i\alpha Pe\bar{w}$ and $L_6 = [(\eta - 1)\bar{\sigma} + 1]\mathscr{L} + (\eta - 1)(D\bar{\sigma})D$. The operator $D = d/dr$ and $\mathscr{L} = D^2 + D/r - m^2/r^2 - \alpha^2$. After imposing the boundary conditions at the centreline $r = 0$ and the wall $r = 1$, the general eigenvalue problem is solved by the standard MATLAB subroutine EIG (Schmid & Henningson 2001).

The convergence of our numerical method is tested here, see table 2. In the work of Selvam *et al.* (2007), 251 Chebyshev collocation points were used to achieve high numerical accuracy without using the technique of clustering the points into the interfacial region, which is quite time consuming. They modified their numerical method by clustering the collocation points into the interfacial region in their further study (Selvam *et al.* 2009). Another test is made by considering a special case: $\eta = 1$, see table 3. The results in table 3 also agree with the results of SH since this special case corresponds to a single fluid flow. They also demonstrate that our numerical method is valid.

REFERENCES

BAYGENTS, J. C. & BALDESSARI, F. 1998 Electrohydrodynamic instability in a thin fluid layer with an electrical conductivity gradient. *Phys. Fluids* **10**, 301–311.

CHANG, M. H., RUO, A. C. & CHEN, F. 2009 Electrohydrodynamic instability in a horizontal fluid layer with electrical conducivity gradient subject to a weak shear flow. *J. Fluid Mech.* **634**, 191–215.

CHEN, C., LIN, H., LELE, S. K. & SANTIAGO, J. G. 2005 Convective and absolute electrokinetic instability with conductivity gradients. *J. Fluid Mech.* **524**, 263–303.

CONROY, D., CRASTER, R., MATAR, O. & PAPAGEORGIOU, D. 2010 Dynamics and stability of an annular electrolyte film. *J. Fluid Mech.* **656**, 481–506.

CONROY, D., MATAR, O., CRASTER, R. & PAPAGEORGIOU, D. 2011 Breakup of an electrified jet with charged surfactants. *Phys. Fluids* **23**, 022103.

CONROY, D., MATAR, O., CRASTER, R. & PAPAGEORGIOU, D. 2012 Compound viscous thread with electrostatic and electrokinetic effects. *J. Fluid Mech.* **701**, 171–200.

DING, Z. & WONG, T. N. 2014 Electrohydrodynamic instability in an annular liquid layer with conductivity gradients. *Phys. Rev.* E **89**, 033010.

DING, Z., WONG, T. N. & LI, H. 2013 Stability of two immiscible leaky-dielectric liquids subjected to a radial electric field in an annulus duct. *Phys. Fluids* **25**, 124103.

GEORGIOU, E., PAPAGEORRIOU, D. T., MALDARELLI, C. & RUMSCHITZKI, D. S. 1991 The double layer–capillary stability of an annular electrolyte film surrounding a dielectric-fluid core in a tube. *J. Fluid Mech.* **226**, 149–174.

GOVINDARAJAN, R. 2004 Effect of miscibility on the linear instability of two-fluid channel flow. *Intl J. Multiphase Flow* **30**, 1177–1192.

GOVINDARAJAN, R., L'VOV, V. S. & PROCACCIA, I. 2001 Retardation of the onset of turbulence by minor viscosity contrasts. *Phys. Rev. Lett.* **87**, 174501.

HOHMAN, M., SHIN, M., RUTLEDGE, G. & BRENNER, M. 2001 Electrospinning and electrically forced jets. I. Stability theory. *Phys. Fluids* **13**, 2201.

KHORRAMI, M. 1991 A Chebyshev spectral collocation method using a staggered grid for the stability of cylindrical flows. *Intl J. Numer. Meth. Fluids* **12**, 825–833.

LIN, H. 2009 Electrokinetic instability in microchannel flows: a review. *Mech. Res. Commun.* **36**, 33–38.

LIN, H., STOREY, B. D., ODDY, M. H., CHEN, C. H. & SANTIAGO, J. G. 2004 Instability of electrokinetic microchannel flows with conductivity gradients. *Phys. Fluids* **16**, 1922–1935.

MELCHER, J. 1981 *Continuum Electromechanics*. MIT.

MELCHER, J. & FIREBAUGH, M. 1967 Travelling-wave bulk electro convection induced across a temperature gradient. *Phys. Fluids* **10**, 1178–1185.

MELCHER, J. & SCHWARTZ, W. 1968 Interfacial relaxation overstability in a tangential electric field. *Phys. Fluids* **11**, 2604–2616.

MELCHER, J. & SMITH, C. 1969 Electrohydrodynamic charge relaxation and interfacial perpendicular-field instability. *Phys. Fluids* **12**, 778–790.

MELSTEL, A. 1996 Electrohydrodynamic stability of a highly viscous jet. *J. Fluid Mech.* **312**, 311–326.

D'OLCE, M., RAKOTOMALALA, N., SALIN, D. & TALON, L. 2008 Pearl and mushroom instability patterns in two miscible fluids' core annular flow. *Phys. Fluids* **20**, 024104.

D'OLCE, M., RAKOTOMALALA, N., SALIN, D. & TALON, L. 2009 Convective/absolute instability in miscible core–annular flow. Part 1. Experiments. *J. Fluid Mech.* **618**, 305–322.

OZEN, O., AUBRY, N., PAPAGEORGIOU, D. T. & PETROPOULOS, P. G. 2006 Monodisperse drop formation in square microchannels. *Phys. Rev. Lett.* **96**, 144501.

RUO, A. C., CHANG, M. H. & CHEN, F. 2010 Effect of rotation on the electrohydrodynamic instability of a fluid layer with an electrical conductivity gradient. *Phys. Fluids* **22**, 024102.

SANTOS, J. J. & STOREY, B. D. 2008 Instability of electro-osmotic channel flow with streamwise conductivity gradients. *Phys. Rev.* E **78**, 046316.

SAVILLE, D. A. 1997 Electrohydrodynamics: the Taylor–Melcher leaky dielectric model. *Annu. Rev. Fluid.* **29**, 27–64.

SCHMID, P. & HENNINGSON, D. 2001 *Stability and Transition in Shear Flows*. Springer.

SELVAM, B., MERK, S., GOVINDARAJAN, R. & MEIBURG, E. 2007 Stability of miscible core–annular flows with viscosity stratification. *J. Fluid Mech.* **592**, 23–49.

SELVAM, B., TALON, B., LESSHAFFT, L. & MEIBURG, E. 2009 Convective/absolute instability in miscible core–annular flow. Part 2. Numerical simulations and nonlinear global modes. *J. Fluid Mech.* **618**, 323–348.

SINTON, D. & LI, D. 2003 Electroosmotic velocity profiles in microchannels. *Colloids Surf.* A **222**, 273–283.

STOREY, B. D., LIN, H. & SANTIAGO, J. G. 2005 Electrokinetic instabilities in thin microchannels. *Phys. Fluids* **17**, 018103.

TALON, L. & MEIBURG, E. 2011 Plane Poiseuille flow of miscible layers with different viscosities: instabilities in the Stokes flow regime. *J. Fluid Mech.* **686**, 484–506.

TAYLOR, G. I. 1966 Studies in electrohydrodynamics. I. The circulation produced in a drop by an electric field. *Proc. R. Soc. Lond.* A **291**, 159–166.

WANG, Q. M. 2012 Breakup of a poorly conducting liquid thread subject to a radial electric field at zero Reynolds number. *Phys. Fluids* **24**, 102102.

YOSHIKAWA, H. N., CRUMEYROLLE, O. & MUTABAZI, I. 2013 Dielectrophoretic force-driven thermal convection in annular geometry. *Phys. Fluids* **25**, 024106.